ELSEVIER

Materials Science and Engineering A 481–482 (2008) 3–10

MATERIALS SCIENCE & ENGINEERING A

www.elsevier.com/locate/msea

Analysis of neutron diffraction spectra acquired *in situ* during mechanical loading of shape memory NiTiFe at low temperatures

V.B. Krishnan [a], R.M. Manjeri [a], B. Clausen [b], D.W. Brown [b], R. Vaidyanathan [a,*]

[a] *Advanced Materials Processing and Analysis Center (AMPAC), Department of Mechanical, Materials and Aerospace Engineering, University of Central Florida, Orlando, FL 32816, USA*

[b] *Los Alamos National Laboratory, Los Alamos, NM 87545, USA*

Received 31 October 2006; accepted 2 November 2006

Abstract

The Spectrometer for Materials Research at Temperature and Stress (SMARTS) at Los Alamos National Laboratory was used to acquire neutron diffraction spectra *in situ* during mechanical loading at 216 and 237 K. The experiments were performed with the objective of following the texture, strain and phase fraction evolution in the trigonal R-phase in a $Ni_{46.8}Ti_{50}Fe_{3.2}$ shape memory alloy. A methodology to quantify the textures, strains and phase fractions using the General Structure Analysis System (GSAS) for Rietveld refinement of neutron diffraction spectra, is implemented and described. Emphasis is placed on evaluating the choice of $P3$ and $P\bar{3}$ space groups for the R-phase in the refinements and the impact of this choice on the quantitative analyses of spectra.

Keywords: NiTiFe shape memory alloy; Phase transformation; Neutron diffraction; Rietveld refinement; R-phase

1. Introduction

Shape memory alloys are incorporated as actuator elements due to their inherent ability to sense a change in temperature and actuate against external loads by undergoing a shape change, as a result of a temperature-induced phase transformation [1–4]. Among various alloy classes, NiTi-based shape memory alloys are more often used due to an advantageous combination of material properties and shape memory behavior [1,5,6]. However, the B19′ monoclinic (martensite) to B2 cubic (austenite) phase transformation associated with shape memory phenomenology in binary NiTi alloys exhibits hysteresis (usually between 1.5 and 145 K) and typically occurs around 50–70 K above or below ambient temperature. The addition of Fe to the NiTi system suppresses the martensitic transformation temperature and stabilizes an intermediate trigonal R-phase. The R-phase transformation in NiTiFe alloys offers a useful window for low temperature actuator operation while exhibiting reduced transformation hysteresis and a favorable fatigue response [7]. In order to better utilize the R-phase transformation in actuator design there is a need to understand fundamental deformation mechanisms associated with it. Such an understanding can be aided tremendously by the use of advanced mechanical characterization techniques.

Among available advanced techniques, *in situ* neutron diffraction at stress and temperature is uniquely suited to following the texture, strain and phase fraction evolution in a bulk polycrystalline shape memory alloy sample [8–11]. Whereas, both neutrons and X-rays (from conventional laboratory sources) can be used for materials characterization, neutrons can penetrate further (several mm) in to the sample and can thus provide insights that are representative of bulk behavior. Crystal structures, residual strains, phase fractions (in multi-phase systems) and textures are among the breadth of information that can be obtained using this technique. The theory of neutron diffraction and its application in materials characterization can be found in Refs. [12–14].

Neutron diffraction measurements have routinely been performed during *in situ* loading at ambient and high temperatures [12,14]. However, there have previously been no measurements performed during loading at cryogenic temperatures. With the objective of investigating deformation in the R-phase, a capa-

* Corresponding author. Tel.: +1 407 882 1180; fax: +1 407 882 1462.
E-mail address: raj@mail.ucf.edu (R. Vaidyanathan).

0921-5093/$ – see front matter © 2007 Elsevier B.V. All rights reserved.
doi:10.1016/j.msea.2006.11.176

bility for *in situ* neutron diffraction during loading at cryogenic temperatures was implemented at Los Alamos National Laboratory for the first time and is outlined in a subsequent section. In theory, the accuracy and completeness of texture, strain and phase fraction measurements increase with the number of measurement orientations and/or detector area coverage. However, in practice, difficulties arise in accurately orienting large samples with auxiliary equipment (e.g., load frame and vacuum chamber), from "shadows" cast from such equipment and from errors associated with sample shifts and changes in the diffraction sampling volume. As a result of the aforementioned considerations, the present study was conducted on the Spectrometer for Materials Research at Temperature and Stress (SMARTS) diffractometer at Los Alamos National Laboratory utilizing a polychromatic beam from a spallation neutron source with detectors in two fixed orientations. There is then a need to establish a methodology to quantitatively follow the strain, texture and phase fraction evolution with this limited detector area coverage. The objective of this paper is to establish such a methodology using Rietveld refinement of neutron spectra (in the General Structure Analysis System (GSAS) [15]) that is not merely focused on structure identification (like, e.g., a transmission electron microscopy investigation would) but uniquely includes the combined analyses of strain, texture and phase fraction information representative of the bulk in the sample. Here we note that such a methodology has previously been established for the cubic phase in NiTi [9] but is now done here for the trigonal phase.

2. Rietveld refinement

Rietveld refinement was originally introduced for the analysis of constant wavelength neutron diffraction data [16,17] and was subsequently used for the refinement of X-ray diffraction patterns in the late 1970s. With rapid increases in computational power, the Rietveld technique is now widely used for the analysis of neutron, X-ray and synchrotron diffraction data. In Rietveld analysis, a least squares method is used to obtain the best possible fit between the complete measured or acquired pattern and a corresponding calculated pattern. Based on the crystal structure of the material being refined, the intensity, Y_{ci}, can be calculated at every point in the spectrum and the position of the observed lattice reflections can be predicted. The calculated intensity depends on numerous factors and can be determined from the expression [18]:

$$Y_{ci} = s\sum_{K} L_K |F_K|^2 \phi(2\theta_i - 2\theta_K) P_K A + Y_{bi} \quad (1)$$

where s is the scaling factor, K the triplet of h, k, and l Miller indices for a Bragg reflection, L_K includes the Lorentz, polarization and multiplicity factors, F_K the structure factor, ϕ the reflection profile function, $2\theta_i$ the observed position of the Bragg peak, $2\theta_K$ the calculated position of the Bragg peak corrected for the zero-point error in the detector, P_K the preferred orientation function, A an absorption factor and Y_{bi} is the background intensity at the ith step of the iteration process. Thus, in order to obtain a good fit between the experimental and calculated patterns, a number of atom position, thermal, site occupancy, lattice, background, instrumental and profile parameters are typically refined, among others. The profile function may include effects from microstrain and crystallite size related peak broadening, specimen and instrument source and geometry. The presence of preferred orientation necessitates the refinement for texture. For example in GSAS, two different models are used for the refinement of texture. The first, following the formulation of March and Dollase [19,20], uses a cylindrical symmetrical version of an ellipsoidal model to describe texture. The second uses a generalized spherical-harmonic [21] description of the orientation distribution function. However, earlier studies have shown that the March–Dollase texture formulation is inadequate to account for evolving texture during martensitic transformations [9]. Accordingly, the generalized spherical-harmonic formulation is preferred over the March–Dollase formulation in this work. The sequence and/or number of parameters being simultaneously refined can influence whether the least square minimization algorithm settles in a local minimum as opposed to a global minimum. Thus, in order to avoid arriving at such false minima [18], there is a need to both quantitatively and qualitatively evaluate the accuracy of the refinement. A qualitative check may include visual inspections as well as ensuring that the model considered has all the necessary parameters to describe both structural and diffraction effects. A quantitative check may utilize representative statistical parameters. Such statistical parameters include crystallographic residual factors (R_{wp}, R_p, etc.) and goodness of fit (χ^2) that can help judge the quality of the fit [15].

3. Experimental procedure

3.1. Sample

A $Ni_{46.8}Ti_{50}Fe_{3.2}$ billet (nominal composition), fabricated by vacuum-induction-melting and vacuum-arc-remelting, was procured from Special Metals, NY. Cylindrical samples of 10 mm diameter by 24 mm length were cut from the billet by electrical discharge machining (EDM) for the neutron diffraction measurements. The samples were then solutionized at 1023 K for 1 h in a vacuum furnace and immediately oil quenched to room temperature. Differential scanning calorimetry at a rate of 0.33 K s^{-1} under nitrogen cover gas was used to determine the start and finish of the R-phase transformation from austenite and the corresponding reverse transformation to austenite from the R-phase. These temperatures were determined to be 236, 223, 227 and 239 ± 2 K, respectively. The transformation to martensite was below 120 K and was hence outside the operating range of the calorimeter used.

3.2. Neutron diffraction and low temperature loading

The neutron diffraction measurements were conducted on the Spectrometer for Materials Research at Temperature and Stress (SMARTS), a third generation neutron diffractometer at Los Alamos National Laboratory [22]. SMARTS has two banks

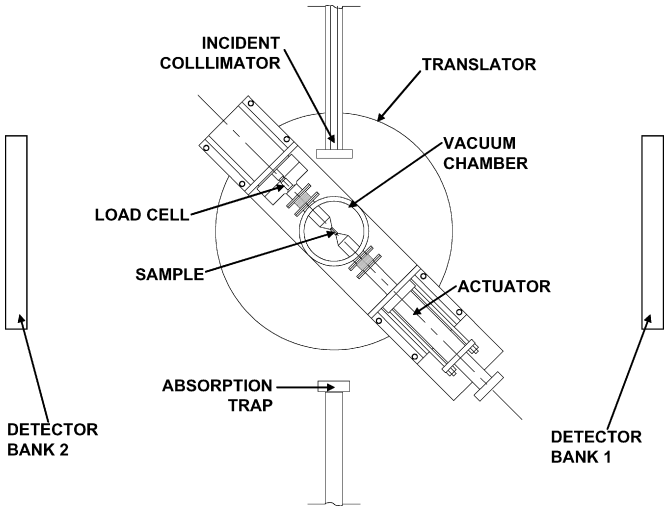

Fig. 1. Schematic of the SMARTS diffractometer with a newly implemented cryogenic loading capability (top view).

of detectors—Bank 1 oriented for measurements from lattice planes whose normals are perpendicular to the loading axis and Bank 2 oriented for measurements from lattice planes whose normals are parallel to the loading axis. The load frame and high temperature vacuum furnace facilitate research on materials under selected combinations of high loads (250 kN) and high temperatures (1773 K). Recently, a cryogenic loading capability (Fig. 1) principally developed for the study of NiTiFe shape memory alloys, was incorporated on the SMARTS diffractometer [23]. With the new cryogenic setup, samples can be cooled to temperatures as low as 90 K during mechanical loading. Neutron diffraction spectra were collected under three experimental conditions in this study:

(i) At 216 K, under a compressive stress of 30 MPa.
(ii) At 216 K, under a compressive stress of 313 MPa.
(iii) At 237 K, under a compressive stress of 44 MPa.

The accumulated count time in each of the above experiments was 19 min or more (23, 19 and 27 min, respectively) at a nominal beam current of 100 μA in order to obtain adequate intensity from a diffraction volume of about 1 cm^3.

4. Results and discussion

4.1. Rietveld refinement

As justified in a subsequent section, the initial structural parameters for the refinement were taken from Refs. [24,25] and the following general methodology implemented in GSAS in the order indicated:

(i) Lattice parameters were refined following the introduction of space groups, histograms and atom parameters (initial atom positions, fractional occupancies and thermal factors). This was followed by a refinement of absorption coefficients. For the two-phase specimen, a constraint (sum adding to unity) was imposed for the refinement of phase fractions.
(ii) The profile coefficients, including the Gaussian variance, isotropic strain and anisotropic strain fitting parameters were then refined. The profile function that fitted the data best was a convolution of two back-to-back exponentials with a Gaussian. The profile coefficients were initially refined independently and subsequently refined simultaneously with the lattice parameter. In the presence of strain (i.e., the externally loaded condition), the strain fitting parameters were refined first and then the variance. For cases where the quantitative determination of strain was the objective, the isotropic and anisotropic strain fitting parameters were not refined, but instead only the lattice parameter and the variance were refined.
(iii) In the next step, the presence of texture was accounted for by the use of a generalized spherical harmonic description of the orientation distribution function [21]. To begin with, the sample orientation relative to the incident neutron and detector banks was appropriately considered. Additionally, the order of the harmonic was considered in an incremental manner such that the order used did not statistically improve the refinement with the next higher order.
(iv) Following the introduction of texture, the profile parameters were refined again, which were followed by refinements of the thermal parameters and atom positions.
(v) Finally, zero-point error/sample height problems were corrected if necessary.

4.2. Phase identification

Based on the DSC results, as expected, the phase transformation to the R-phase was complete under the first two experimental conditions at 216 K. The stresses of 30 and 313 MPa resulted in elastic deformation of the R-phase and not a stress-induced transformation of the R-phase to B19′ martensite. From the DSC measurements, the reverse transformation from the R-phase to austenite was expected to start at 227 K and finish at 239 K. However, under a compressive stress of 44 MPa at 237 K (the third experimental condition), the transformation is expected to finish at a temperature higher than 239 K, which results in a substantial amount of the R-phase remaining at 237 K as it transforms to the B2 austenite. A summary of the phases present under the three experimental conditions is shown in Table 1.

4.3. Structure identification

The R-phase is considered to be derived from a rhombohedral distortion of the parent, cubic B2 austenite phase [26–28].

Table 1
Experimental conditions and the corresponding phases present

Experimental condition	Temperature (K)	Stress (MPa)	Phase
1	216	30	R-phase
2	216	313	R-phase
3	237	44	R-phase + austenite

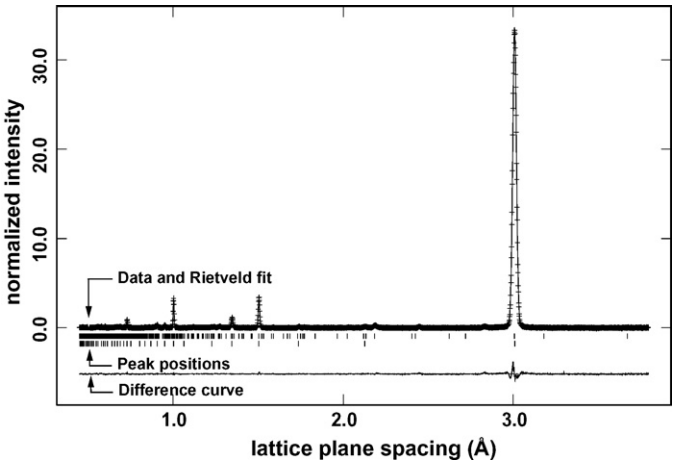

Fig. 2. A typical GSAS Rietveld refinement output with the R-phase refined as belonging to the $P3$ space group (for spectrum obtained from the sample under a compressive stress of 44 MPa at 237 K) for diffracting lattice planes whose normals are parallel to the loading axis. The measured data are indicated by cross-marks and the calculated profile is indicated by the solid-line curve. The line-marks below the profile pattern indicate the positions of all possible Bragg reflections. The lower graph shows the difference between the measured and calculated profile patterns.

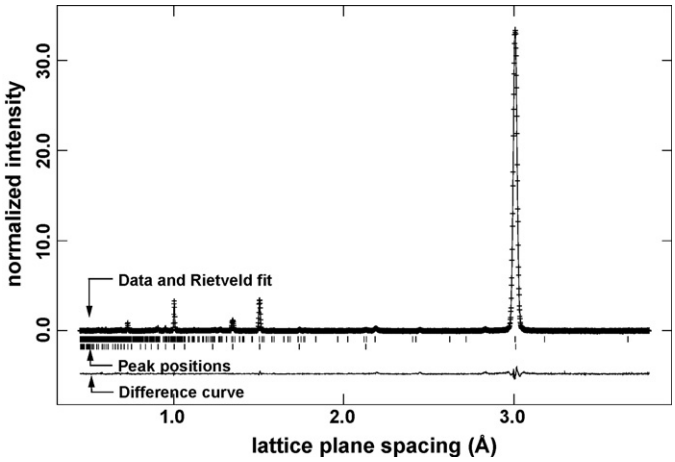

Fig. 3. A typical GSAS Rietveld refinement output with the R-phase refined as belonging to the $P\bar{3}$ space group (for spectrum obtained from the sample under a compressive stress of 44 MPa at 237 K) for diffracting lattice planes whose normals are parallel to the loading axis. The measured data are indicated by cross-marks and the calculated profile is indicated by the solid-line curve. The line-marks below the profile pattern indicate the positions of all possible Bragg reflections. The lower graph shows the difference between the measured and calculated profile patterns.

However, the structure of the R-phase has been under debate for some time. Substantial research has been done in determining the crystal structure of the R-phase using a variety of characterization techniques such as X-ray diffraction (XRD), transmission electron microscopy (TEM), synchrotron diffraction and neutron diffraction [24,25,29–34]. Hara et al. [31] suggest the space group $P3$, employing convergent beam electron diffraction (CBED), electron diffraction considering dynamic scattering and X-ray diffraction using Rietveld analyses. Schryvers and Potapov [29] utilized nanoprobe electron diffraction patterns and recommended the space group $P\bar{3}$ rather than the space group $P3$, even though they obtained better results with the space group $P3$. While considering the interatomic distances between constituent atoms, they claim that the variation in the interatomic distances is smaller by choosing space group $P\bar{3}$ over space group $P3$. More recently, Sitepu et al. [33] and Khalil-Allafi et al. [34] obtained better results with $P\bar{3}$ while using synchrotron and neutron diffraction data that were refined by the Rietveld method.

Given the ambiguity, both space groups $P\bar{3}$ and $P3$ were considered in Rietveld refinement of spectra obtained in this study under the various experimental conditions. Fig. 2 shows a representative GSAS Rietveld refinement output (for spectrum obtained from the sample under a compressive stress of 44 MPa at 237 K) using the space group $P3$ for the R-phase in the presence of austenite. Fig. 3 is the corresponding output for the R-phase with the space group $P\bar{3}$. The atom positions were also refined for each of the three experimental conditions. Tables 2 and 3 show results from refining atom positions using space groups $P3$ and $P\bar{3}$, respectively. The comparative results of evaluating the refinement for space groups $P3$ and $P\bar{3}$ in terms of refinement quality of fit parameters (χ^2, R_{wp} and R_p) are given in Table 4. The refinement quality of fit parameters for all three experimental conditions do not show notable differences between space groups $P3$ and $P\bar{3}$.

4.4. Texture determination

A generalized spherical harmonic description of the orientation distribution function was used to account for the evolving texture in the R-phase and the processing induced texture in the parent B2 austenite phase. At the outset we note that refining

Table 2
R-phase atom positions for the three experimental conditions, refined with the R-phase belonging to the $P3$ space group

Atom positions	Refined parameters	216 K, 30 MPa	216 K, 313 MPa	237 K, 44 MPa
Ti 1(0, 0, 0)	–	–	–	–
Ti 2(1/3, 2/3, z)	z	0.0792	0.0817	0.0740
Ti 3(2/3, 1/3, z)	z	0.121	0.0227	0.0065
Ti 4(x, y, z)	x	0.3328	0.3345	0.3375
	y	−0.0056	−0.0046	−0.0020
	z	0.3618	0.3611	0.3545
Ti 5(x, y, z)	x	0.6753	0.6784	0.6748
	y	0.0094	0.0094	0.0128
	z	0.6838	0.6868	0.6825
Ni 1(0, 0, z)	z	0.4710	0.4685	0.4690
Ni 2(1/3, 2/3, z)	z	0.5510	0.5483	0.5421
Ni 3(2/3, 1/3, z)	z	0.4204	0.4183	0.4274
Ni 4(x, y, z)	x	0.3186	0.3191	0.3199
	y	−0.0211	−0.0207	−0.0227
	z	0.8580	0.8582	0.8572
Ni 5(x, y, z)	x	0.6858	0.6861	0.6850
	y	0.0194	0.0200	0.0189
	z	0.1593	0.1605	0.1582

Table 3
R-phase atom positions for the three experimental conditions, refined with the R-phase belonging to the $P\bar{3}$ space group

Atom positions	Refined parameters	216 K, 30 MPa	216 K, 313 MPa	237 K, 44 MPa
Ti 1(0, 0, 0)	–	–	–	–
Ti 2(1/3, 2/3, z)	z	0.0280	0.0290	0.0236
Ti 3(x, y, z)	x	0.3321	0.3313	0.3312
	y	−0.0070	−0.0083	−0.0069
	z	0.3417	0.3416	0.3441
Ni 1(0, 0, 1/2)	–	–	–	–
Ni 2(1/3, 2/3, z)	z	0.5643	0.5622	0.5589
Ni 3(x, y, z)	x	0.3225	0.3228	0.3219
	y	−0.0194	−0.0188	−0.0199
	z	0.8527	0.8539	0.8556

for texture despite limited detector area coverage may in some cases merely serve to improve the quality of the refinement rather than represent crystallographic phenomena. Incorporating data from both detectors and accounting for cylindrical symmetry in the sample, a 24th order spherical-harmonic description was used. This order was arrived at by iterating from lower orders and qualitatively/quantitatively examining the refinement, until increasing the order of the harmonic did not improve the refinement.

The quantification of texture can be defined by a single parameter, the texture index J [35]:

$$J = \oint [f(g)]^2 \, \mathrm{d}g \tag{2}$$

where $f(g)$ is the orientation distribution function that maps the probability of each of the possible grain orientations with respect to the external sample dimensions and the integration is over all orientation space. J lies between unity and infinity, corresponding to random orientations and to a single crystal, respectively. The texture index of the R-phase was 19.4 using the space group $P3$ and 25.2 with the space group $P\bar{3}$ for the measurements at 216 K, under a compressive stress of 30 MPa. Correspondingly, the texture index was 35.7 using the space group $P3$ and 42.1 with the space group $P\bar{3}$ for the measurements at 216 K, under a compressive stress of 313 MPa. However, for the measurement at 237 K (where both R-phase and austenite co-exist), the space group $P\bar{3}$ resulted in an unrealistic texture index when compared to normalized spectra as discussed in a later section.

The space group $P3$ has the lowest possible symmetry in the trigonal system, while space group $P\bar{3}$ has a center of symmetry.

Table 4
Quality of fit parameters [15] for the two sets of Rietveld refinements ($P3$ and $P\bar{3}$)

Experimental condition	$P3$			$P\bar{3}$		
	χ^2	R_{wp}	R_p	χ^2	R_{wp}	R_p
216 K, 30 MPa	4.495	4.88	3.61	4.586	4.93	3.63
216 K, 313 MPa	4.566	5.48	4.07	4.645	5.53	4.07
237 K, 44 MPa	5.318	5.36	3.67	5.640	5.52	3.86

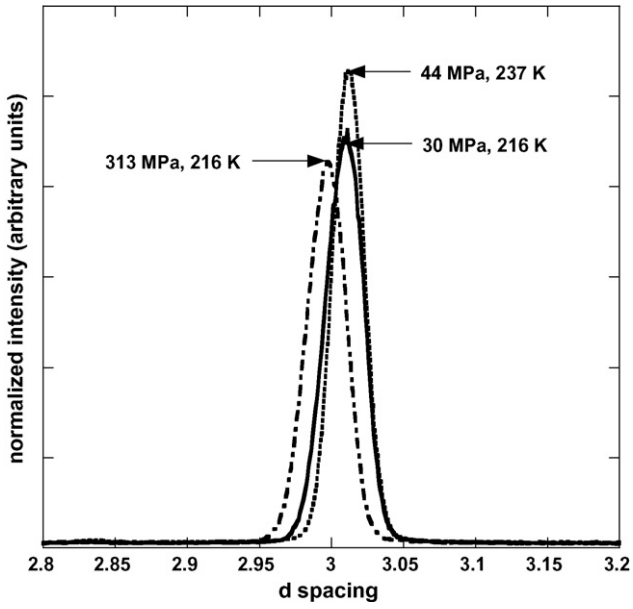

Fig. 4. Section of normalized neutron diffraction spectra corresponding to R-phase {1 1 1} lattice plane reflections (most intense) for the various experimental conditions. The reflections shown here are from diffracting lattice planes whose normals are parallel to the loading axis.

By using electron diffraction data from small single crystalline R-phase regions, Schryvers and Potapov [29] demonstrated that atoms in the R-phase are located in centrosymetric positions thus belonging to the space group $P\bar{3}$ rather than the space group $P3$. This may be true considering that the diffraction measurements represented single crystalline regions. However, for the case of neutron diffraction, the measurements are representative of much larger polycrystalline areas. Following preferential phase transformation (i.e., some variants of R-phase transforming earlier to austenite when compared to others) in the bulk, a heterogeneous strain distribution may result that causes a loss of the center of symmetry. This has previously been reported for ferroelectric metals [36,37]. The space group $P3$ rather than the space group $P\bar{3}$ better captures this loss of center of symmetry. This may explain the unrealistically high texture index for a fit with the space group $P\bar{3}$.

Figs. 4 and 5 represent the normalized intensities of the two most intense peak reflections for the three experimental conditions. The most intense peak corresponds to the {1 1 1} planes, while the less intense peak corresponds to the {4 1 1} and {5 $\bar{1}$ 1} planes. It can be seen that the intensity of the first peak decreases while that of the second peak increases with external loading, representative of texture evolution. Furthermore, during the phase transformation at 237 K, the changes in intensities are relatively higher showing substantial texture evolution. The texture evolution in the sample can be represented by the texture index as well as axial distribution plots. While the texture index is merely a number that represents trends in the texture evolution, a more detailed representation is given by axial distribution plots. In an axial distribution plot, the y-axis is a measure of the number of grains that are at an angle ϕ between the normal to the chosen plane and the loading axis (in this case), compared to a randomly oriented

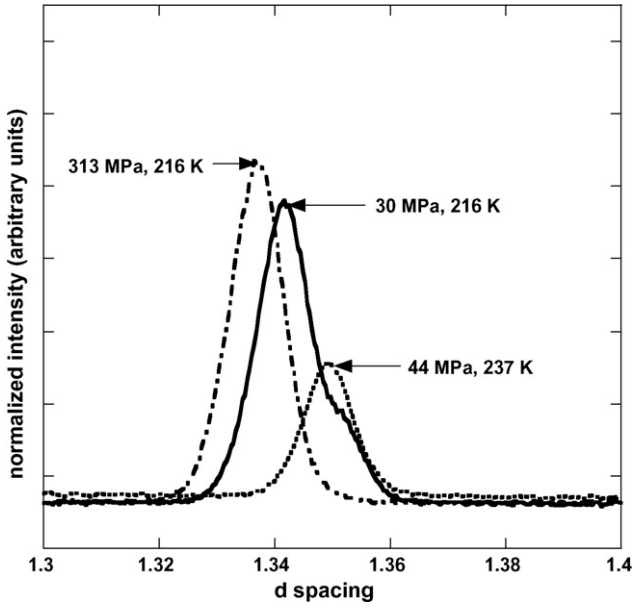

Fig. 5. Section of normalized neutron diffraction spectra corresponding to R-phase $\{4\,1\,1\}$ and $\{5\,\bar{1}\,1\}$ lattice plane reflections (second most intense) for the various experimental conditions. The reflections shown here are from diffracting lattice planes whose normals are parallel to the loading axis.

polycrystal. Thus, a random polycrystalline sample would be represented by a horizontal line at unity. There is no physical significance associated with values of less than zero, which in these plots is an outcome of the global normalization procedure. Figs. 6 and 7 show the axial distribution plots of the $(1\,1\,\bar{1})$ plane for all the three experimental conditions, using both space groups $P3$ and $P\bar{3}$, respectively. Again here, the choice of the space group $P\bar{3}$ unrealistically overestimates the strength of the texture when correlated with individual peak reflections in Fig. 4.

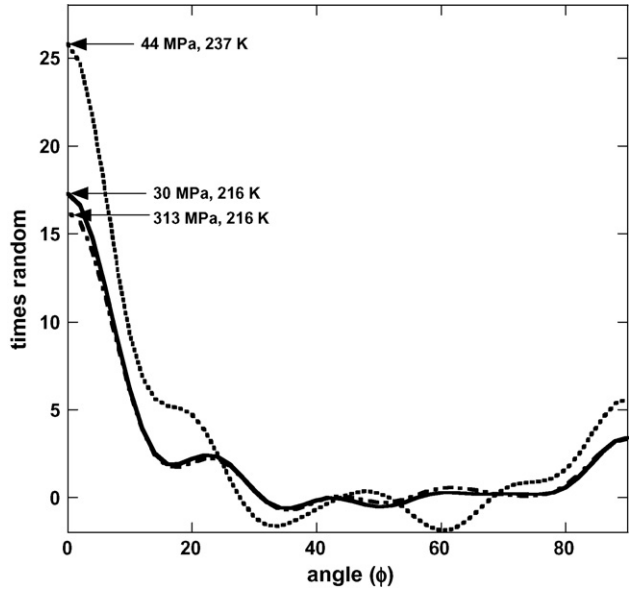

Fig. 6. R-phase $(1\,1\,\bar{1})$ axial distribution plots (refined as belonging to the $P3$ space group) for the various experimental conditions. ϕ is the angle between the $(1\,1\,\bar{1})$ plane normal and the loading axis.

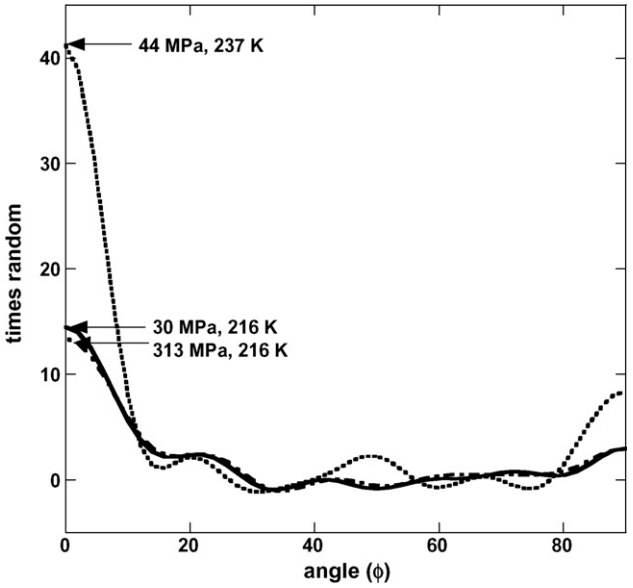

Fig. 7. R-phase $(1\,1\,\bar{1})$ axial distribution plots (refined as belonging to the $P\bar{3}$ space group), for the various experimental conditions. ϕ is the angle between the $(1\,1\,\bar{1})$ plane normal and the loading axis.

4.5. Strain determination

The shift in peak positions represents (elastic) lattice strains and can be measured from either single peak fitting or lattice parameter refinement from the Rietveld method. The single peak method relies on fitting each $h\,k\,l$ plane individually for the lattice spacing, $d^{h\,k\,l}$. The strain for a specific $h\,k\,l$ plane is then given by:

$$\varepsilon_{h\,k\,l} = \frac{d^{h\,k\,l} - d_0^{h\,k\,l}}{d_0^{h\,k\,l}} \tag{3}$$

where $d_0^{h\,k\,l}$ is the corresponding "strain free" spacing. The three most intense peaks were used for single peak fitting, corresponding to the $\{1\,1\,1\}$; $\{4\,1\,1\}$ and $\{5\,\bar{1}\,1\}$; and $\{2\,2\,2\}$ planes, respectively. As previously described, the Rietveld method refines lattice parameters (a and c in this case) that inherently average all the lattice planes that diffract in a particular bank of detectors. For strain determination, the histogram from the Bank 2 detector (representing measurements from lattice planes whose normals are parallel to the axis of loading) was considered and only the variance (among profile coefficients) was refined with the lattice parameter. The lattice parameter obtained from Rietveld refinement was used to obtain the lattice spacings,

Table 5
Strain evaluation using single peak fitting

Lattice planes	$d^{h\,k\,l}$ at 30 MPa (Å)	$d^{h\,k\,l}$ at 313 MPa (Å)	E (GPa)
$\{1\,1\,1\}$	3.0092	2.9969	68
$\{4\,1\,1\}$ and $\{5\,\bar{1}\,1\}$	1.3409	1.3366	87
$\{2\,2\,2\}$	1.5043	1.4981	70

The typical error associated with the d-spacing determination is ± 0.0003.

Table 6
Strain evaluation using the Rietveld approach for the two sets of refinements at 216 K ($P3$ and $P\bar{3}$)

Lattice planes	$P3$			$P\bar{3}$		
	d^{hkl} at 30 MPa (Å) (a = 7.3370 Å, c = 5.2616 Å)	d^{hkl} at 313 MPa (Å) (a = 7.3134 Å, c = 5.2302 Å)	E (GPa)	d^{hkl} at 30 MPa (Å) (a = 7.3371 Å, c = 5.2611 Å)	d^{hkl} at 313 MPa (Å) (a = 7.3140 Å, c = 5.2291 Å)	E (GPa)
{1 1 1}	3.0092	2.9969	68	3.0092	2.9969	68
{4 1 1} and {5 $\bar{1}$ 1}	1.3407	1.3362	83	1.3408	1.3363	85
{2 2 2}	1.5046	1.4984	69	1.5046	1.4984	69

The typical error associated with the lattice parameter determination is ±0.0002.

d^{hkl} of the aforementioned planes from:

$$\frac{1}{(d^{hkl})^2} = \frac{4}{3}\left[\frac{h^2 + hk + k^2}{a^2}\right] + \frac{l^2}{c^2} \quad (4)$$

The strain for a specific hkl plane was then obtained using Eq. (3). This strain, together with the increase in the applied stress, σ^{applied}, was used to determine a plane-specific elastic modulus, E_{hkl}, from:

$$E_{hkl} = \frac{\sigma^{\text{applied}}}{\varepsilon_{hkl}} \quad (5)$$

Tables 5 and 6 show the elastic moduli determined in the aforementioned manner for the measurements at 216 K using both single peak and Rietveld analyses, with space groups $P3$ and $P\bar{3}$, respectively. The results are the same for the lattice reflections considered. Here we note that we have reported moduli from two strain measurements in order to highlight the agreement between single peak and Rietveld approaches for strain determination. These values were checked with additional measurements (not reported here) and remained within error.

4.6. Phase fraction determination

In the presence of additional phases, the refinement for phase fraction involved setting of phase and histogram constraints. During the phase transformation at 237 K, the refinements with $P3$ showed a weight fraction of 44% for austenite (remaining R-phase), while that with $P\bar{3}$ was 38.50 %. These values are within the estimated errors of ±3%. A qualitative inspection of the diffraction spectra along with the thermal history suggested that the presence of austenite was in the range of 30–50% at 237 K. Again, the Rietveld analyses for phase fractions at 237 K using space groups $P3$ and $P\bar{3}$ produced comparable results.

5. Conclusions

The Spectrometer for Materials Research at Temperature and Stress (SMARTS) at Los Alamos National Laboratory was used to acquire neutron diffraction spectra *in situ* during selected combinations of mechanical loading (up to 313 MPa) and cooling (down to 216 K) from a $Ni_{46.8}Ti_{50}Fe_{3.2}$ shape memory alloy. The spectra, representative of bulk measurements in the trigonal R-phase and cubic austenite phase in such an alloy, were subjected to the Rietveld method using GSAS for the quantitative determination of strains, textures and phase fractions. A general methodology for implementing such refinements is described as it applies to cases where the strain, texture and phase fraction simultaneously evolve (e.g., in shape memory alloys under stress and/or temperature changes) and practical limitations arise in terms of detector coverage or measurable sample orientations (arising from the need for auxiliary equipment to mechanically stress and thermally cool the sample simultaneously, while allowing a neutron line of sight). Given an existing ambiguity in the published literature as to whether the trigonal R-phase belongs to the $P3$ or $P\bar{3}$ space groups, Rietveld analyses were separately carried out incorporating the symmetries associated with both space groups and the impact of this choice evaluated. No statistical differences in the refinement quality were noted for structure, strain and phase fraction analyses between the choice of $P3$ or $P\bar{3}$ space groups. The accuracy of the refinement for strain determination was confirmed by comparing single peak fitting and Rietveld approaches which resulted in comparable results for the three sets of reflections considered. The accuracy of the texture and phase fraction determination was confirmed from visual inspection of raw spectra. For texture analyses, the choice of the $P\bar{3}$ space group resulted in unrealistically high texture indices (when compared to qualitative analyses). This was attributed to the heterogeneous strain in the diffracting volume resulting in a loss of the center of symmetry. In summary, this work has thus set the stage for using Rietveld refinement to quantitatively follow the strain, texture and phase fraction evolution in the R-phase of NiTiFe during mechanical loading at low temperatures on the SMARTS neutron diffractometer at Los Alamos National Laboratory.

Acknowledgements

This work has benefited from the use of the Lujan Neutron Scattering Center at LANSCE, which is funded by the Department of Energy's Office of Basic Energy Sciences. Los Alamos National Laboratory is operated by Los Alamos National Security LLC under DOE Contract DE-AC52-06NA25396. The authors are grateful to T. Sisneros (Los Alamos), T. Woodruff, S. Shmalo and C.R. Rathod (rest UCF) for valuable experimental assistance. Financial support from NSF (CAREER DMR-0239512), NASA (NAG3-2751) and SRI is gratefully acknowledged.

References

[1] H. Funakubo, Shape Memory Alloys, Gordon and Breach Science Publishers, New York, 1987.
[2] L.M. Schetky, in: T.W. Duerig, K.N. Melton, D. Stöckel, C.M. Wayman (Eds.), Engineering Aspects of Shape-memory Alloys, Butterworth-Heinemann, London, 1990.
[3] K. Otsuka, C.M. Wayman (Eds.), Shape Memory Materials, Cambridge University Press, 1998, pp. 170–178.
[4] R. Vaidyanathan, Kirk-Othmer Encyclopedia of Chemical Technology, Wiley InterScience, John Wiley & Sons Inc., New York, 2002.
[5] T.W. Duerig, A.R. Pelton, Material Properties Handbook: Titanium Alloys, ASM International, 1994, pp. 1035–1048.
[6] K. Otsuka, X. Ren, Prog. Mater. Sci. 50 (2005) 511.
[7] J.L. Lemanski, V.B. Krishnan, R. Mahadevan Manjeri, W.U. Notardonato, R. Vaidyanathan, Adv. Cryo. Eng. 52 (2006) 3–10.
[8] M.A.M. Bourke, R. Vaidyanathan, D.C. Dunand, Appl. Phys. Lett. 69 (1996) 2477.
[9] R. Vaidyanathan, M.A.M. Bourke, D.C. Dunand, J. Appl. Phys. 86 (1999) 3020.
[10] R. Vaidyanathan, M.A.M. Bourke, D.C. Dunand, Acta Mater. 47 (1999) 3353.
[11] R. Vaidyanathan, D.C. Dunand, U. Ramamurty, Mater. Sci. Eng. A 289 (2000) 208.
[12] M.A.M. Bourke, J.A. Goldstone, T.M. Holden, in: M.T. Hutchings, A.D. Krawitz (Eds.), Measurement of Residual and Applied Stress Using Neutron Diffraction, NATO ASI Series E, vol. 216, Kluwer, 1992.
[13] M.T. Hutchings, P.J. Withers, T.M. Holden, T. Lorentzen (Eds.), Introduction to the Characterization of Residual Stress by Neutron Diffraction, Taylor & Francis, 2005.
[14] M.E. Fitzpatrick, A. Lodini (Eds.), Analysis of Residual Stress by Diffraction Using Neutron and Synchrotron Radiation, Taylor & Francis, 2003.
[15] A.C. Larson, R.B. Von Dreele, General Structure Analysis System (GSAS), Los Alamos National Laboratory LAUR 8-748 (1986).
[16] H.M. Rietveld, Acta Crystallogr. 20 (1966) 508.
[17] H.M. Rietveld, Acta Crystallogr. 21 (1966) A228.
[18] R.A. Young (Ed.), The Rietveld Method, Oxford University Press, 1995.
[19] A. March, Z. Krystallogr. 81 (1932) 285.
[20] W.A. Dollase, J. Appl. Crystallogr. 19 (1986) 267.
[21] H.J. Bunge, Texture Analysis in Materials Science, Butterworth-Heinemann, 1982.
[22] M.A.M. Bourke, D.C.E. Dunand, E. Üstündag, Appl. Phys. A 74 (2002) S1707.
[23] T. Woodruff, V.B. Krishnan, B. Clausen, D. Brown, T. Sisneros, M.A.M. Bourke, R. Vaidyanathan, Rev. Sci. Instrum., submitted for publication.
[24] T. Hara, T. Ohba, K. Otsuka, J. de Physique III 5 (1995) 641.
[25] H. Sitepu, Textures and Microstructures 35 (2003) 185.
[26] V.N. Khachin, Y.I. Paskal, V.E. Gunter, A.A. Monasevich, V.P. Sivokha, Phys. Met. Metallogr. (1978) 46.
[27] H.C. Ling, R. Kaplov, Metall. Trans. A 11 (1980) 77.
[28] M.B. Salamon, M.E. Meichle, C.M. Wayman, Phys. Rev. B 31 (1985) 7306.
[29] D. Schryvers, P.L. Potapov, Mater. Trans. JIM 43 (2002) 774.
[30] E. Goo, R. Sinclair, Acta Metall. 33 (1985) 1717.
[31] T. Hara, T. Ohba, E. Okunishi, K. Otsuka, Mater. Trans. JIM 38 (1997) 11.
[32] T. Goryczka, H. Morawiec, J. Alloys Compd. 367 (2004) 137.
[33] H. Sitepu, J.P. Wright, T. Hansen, D. Chateigner, H.G. Brokmeier, C. Ritter, T. Ohba, Mater. Sci. Forum 495–497 (2005) 255.
[34] J. Khalil-Allafi, W.W. Schmahl, D.M. Toebbens, Acta Mater. 54 (2006) 3171.
[35] E.F. Sturcken, J.W. Croach, Trans. Metall. Soc. AIME 227 (1963) 934.
[36] P.W. Anderson, E.I. Blount, Phys. Rev. Lett. 14 (1965) 217.
[37] I.A. Sergienko, V. Keppens, M. McGuire, R. Jin, J. He, S.H. Curnoe, B.C. Sales, P. Blaha, D.J. Singh, K. Schwarz, D. Mandrus, Phys. Rev. Lett. 92 (2004), 065501-1.